2019

Manipulation of LIPSS orientation on silicon surfaces using orthogonally polarized femtosecond laser double-pulse trains

Wei Liu

Lan Jiang

Weina Han

Jie Hu

Xiaowei Li

See next page for additional authors

Authors
Wei Liu, Lan Jiang, Weina Han, Jie Hu, Xiaowei Li, Ji Huang, Shenghua Zhan, and Yongfeng Lu

Research Article | Vol. 27, No. 7 | 1 Apr 2019 | OPTICS EXPRESS 9782
Optics EXPRESS

Manipulation of LIPSS orientation on silicon surfaces using orthogonally polarized femtosecond laser double-pulse trains

Wei Liu,[1] Lan Jiang,[1] Weina Han,[2] Jie Hu,[1,*] Xiaowei Li,[1] Ji Huang,[1] Shenghua Zhan,[1] and Yongfeng Lu[3]

[1]*Laser Micro/Nano Fabrication Laboratory, School of Mechanical Engineering, Beijing Institute of Technology, Beijing 100081, China*
[2]*Beijing Engineering Research Center of Applied Laser Technology, Institute of Laser Engineering, Beijing University of Technology, Beijing 100124, China*
[3]*Department of Electrical and Computer Engineering, University of Nebraska-Lincoln, Lincoln, Nebraska 68588-0511, USA*
**jiehu2@bit.edu.cn*

Abstract: Laser-induced periodic surface structures (LIPSS) provide an easy and cost-effective means of fabricating gratings and have been widely studied in recent decades. To overcome the challenge of orientation controllability, we developed a feasible and efficient method for manipulating the orientation of LIPSS in real time. Specifically, we used orthogonally polarized and equal-energy femtosecond laser (50 fs, 800 nm) double-pulse trains with time delay about 1ps, total peak laser fluence about 1.0 J/cm^2, laser repetition frequency at 100 Hz and scanning speed at 150 μm/s to manipulate the LIPSS orientation on silicon surfaces perpendicular to the scanning direction, regardless of the scanning paths. The underlying mechanism is attributed to the periodic energy deposition along the direction of surface plasmon polaritons (SPPs), which can be controlled oriented along the scanning direction in orthogonally polarized femtosecond laser double-pulse trains surface scan processing. An application of structural colors presents the functionality of our method.

1. Introduction

Since their discovery in the 1800s, gratings have been extensively used in devices and applications such as spectrometers [1], solar cells [2], lasers [3], light-emitting diode illumination [4], and bionics [5]. To fabricate adequate gratings, the grating constant and large-scale uniformity must be ensured. Although traditional fabrication methods such as photolithography [6] and mechanical scribing with ruling engines [7] can ensure a suitable grating constant and large-scale uniformity and have been developed over a long time, these methods require complex fabrication processes and expensive devices. Self-organized structures called laser-induced periodic surface structures (LIPSS) have recently been discovered; the periods of such structures can be maintained constant and on the sub micro scale [8], and thus these structures could afford a new strategy for easy and cost-effective grating fabrication. In addition, LIPSS could be fabricated on virtually all materials, including metals [9], semiconductors [10], and dielectrics [11], which considerably expands the application range of gratings. Several parameters limit application of LIPSS, including uniformity, orientation, periodicity, and large-area consistency. In particular, the orientation of LIPSS plays a major role in the application fields. For instance, in holograms and surface color marking, the intensity and color of diffracted light change with the angle between the LIPSS orientation and incident white light. A well-designed LIPSS pattern could transform into a vivid hologram pattern when illuminated by white light [12]. In optical data storage, LIPSS with different orientations could record different types of information [13].

#358614 https://doi.org/10.1364/OE.27.009782
Journal © 2019 Received 25 Jan 2019; revised 10 Mar 2019; accepted 14 Mar 2019; published 22 Mar 2019

Optics EXPRESS

The morphology of LIPSS is usually related to laser processing parameters such as laser fluence [14], total energy input influences [15], laser repetition frequency [16], laser wavelength [17], scanning speed [18], scanning direction [19], use of laser bursts [20], and processing environment [21]. In general, for linear polarized single-pulse femtosecond laser processing on a single spot, the orientation of LIPSS whose period is near the irradiation wavelength on silicon surfaces is determined by the laser polarization and perpendicular to it in most situations [8]. However, this cannot be extended to the surface scan processing, Liu et al. found that the orientation of LIPSS on silicon surfaces was also influenced by scanning direction and speed, and it would rotate by certain angles [19]. In addition, when relating to the single-spot irradiation on silicon surfaces using delayed parallel or orthogonally polarized, single- or two-color double-fs-pulse trains, the factors that determine the orientation of LIPSS could be more complicated. For parallel polarized double-pulse femtosecond laser processing, the orientation of LIPSS is perpendicular to the laser polarization [22]. However, for orthogonally polarized and unequal-energy femtosecond double-pulse laser processing, S. Höhm et al. found that when having time delays, the LIPSS orientation of single-spot irradiation on silicon surfaces was determined by the stronger pulse and was perpendicular to its polarization [23]. F. Fraggelakis et al. found that when time delay was zero, the LIPSS orientation of single-spot irradiation on silicon surfaces was determined by both the two pulses and was perpendicular to the vector addition of the two pulses' polarizations [24]. They also found that the second pulse arrived at the silicon surface determined the LIPSS orientation in the case of equal-energy [24]. For even more complicated case of two-color double-pulse processing, S. Höhm et al. found that the time delay also had influence on the LIPSS orientation on silicon surfaces [25]. The LIPSS orientation was determined by IR-pulse and perpendicular to its polarization when larger time delay (>2 ps) was employed while the LIPSS induced by IR-pulse and UV-pulse coexisted when time delay less than 2 ps.

When applying LIPSS to the fabrication of gratings, surface scan processing is always required. To manipulate LIPSS orientation during surface scan processing, the direction of laser polarization need to be changed. For instance, B. Dusser et al. fabricated a specific color LIPSS pattern of Van Gogh by using a half-wave plate to change the direction of laser polarization [26]. However, precisely and dynamically controlling complex LIPSS orientations in real time remains a major challenge. Special polarization states of radial- or azimuthal-polarized laser beams must be used to achieve complex LIPSS orientations [27,28]. Recent studies have demonstrated that the morphology of LIPSS can be controlled by manipulating the SPPs. For example, T. J. Derrien et al. controlled the area of LIPSS by controlling the "SPPs active area" through double-pulse irradiation [29]. Wang et al. developed a method for rapid fabrication of large-area LIPSS by shaping the excitation region of SPPs into a long ellipse using a cylindrical lens [30]. This effect is based on the SPPs-laser scattering dynamics control, which has been widely accepted as the main mechanism of the LIPSS formation as well as the grating-assisted SPPs-laser coupling enhancement effect [31]. Thus, it is vital to steer the precise control of the SPPs directions, which determine the final processed LIPSS orientations. However, aforementioned traditional method requires the use of complex devices for controlling the laser polarization state and computer programming procedure, rendering it relatively inefficient approach.

In this study, we developed a feasible and effective method for manipulating the orientation of LIPSS on silicon surfaces in real time during surface scan processing. By employing orthogonally polarized and equal-energy femtosecond double-pulse trains with a short time delay, we were able to control the direction of SPPs along the scanning direction; thus, the LIPSS orientation could be controlled to be perpendicular to the scanning direction, regardless of the scanning path (i.e., straight or curved scanning paths). Moreover, by maintaining the time delay between the two sub pulses at approximately 1 ps, LIPSS with adequate uniformity were obtained. The underlying mechanism of the proposed method is

Optics EXPRESS

outlined as follows: the intensity of SPPs was determined to change with the angles between the scanning direction and laser polarization direction; thus, by adding SPPs vectors excited by orthogonally polarized and equal-energy femtosecond double-pulse trains, we could control the direction of SPPs along the scanning direction. To demonstrate the simplicity and superiority of our method, we applied it to generate structural colors; we determined that only one parameter, namely the scanning direction, needing to be adjusted in the application.

2. Experimental setup

A commercial chirped-pulse Ti: sapphire regenerative oscillator–amplifier laser system (Spitfire, Spectra-Physics Inc.) was applied to generate femtosecond laser pulses with a central wavelength of 800 nm, pulse duration of 50 fs and laser repetition frequency of 100 Hz. A Michelson interferometer with a 45°-rotated quarter-wave plate placed in one of its arms was used to produce orthogonally polarized femtosecond double-pulse trains. Executing polarization at other angles simply required rotating the quarter-wave plate by the corresponding angles. Because the polarizing beam splitter (CM1-BP145B2, Thorlabs) used in the experiment had different reflectivity and transmittance for lasers of different polarization directions, two attenuators were placed on the two arms of the Michelson interferometer to ensure that the energies of the two different polarized laser pulses were equal. Polished crystalline silicon with crystal orientation of (1 1 1) was fixed on a six-axis translation stage that could be programmed to move at a constant speed in an arbitrary direction. A 5 × microscope objective lens (NA = 0.15) was used to focus the laser beams onto the sample surface. Figure 1 presents the detailed experimental setup; the dotted box indicates the corresponding scanning paths.

LIPSS formation is triggered when the laser fluence is marginally higher than the material's ablation threshold. In surface patterning, uniform and smooth LIPSS can be obtained by first determining an appropriate laser fluence and then maintaining the effective pulse number at a suitable value by controlling the laser repetition rate and scanning speed. Accordingly, in this study, we first determined an appropriate laser fluence for surface patterning. By measuring the diameter of the ablated spot (D) as a function of the incident pulse energy (E_{in}) [32], we derived a peak single-pulse ablation threshold of 0.52 J/cm^2, which was in agreement with the value reported in a previous study [27], and an on-target Gaussian spot diameter of 9 μm (the laser beam diameter was maintained at 5 mm before the beam entered the objective lens). The laser repetition rate and scanning speed were maintained at 100 Hz and 150 μm/s, respectively. Hence, the number of effective pulses per beam spot diameter was calculated to be approximately 3.8.

Optics EXPRESS

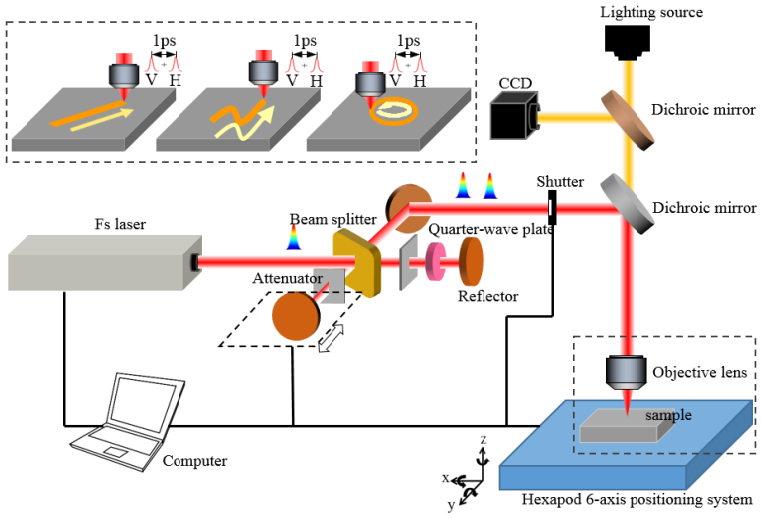

Fig. 1. Experimental setup of fabrication system comprising orthogonally polarized femtosecond laser double-pulse trains.

3. Results and discussion

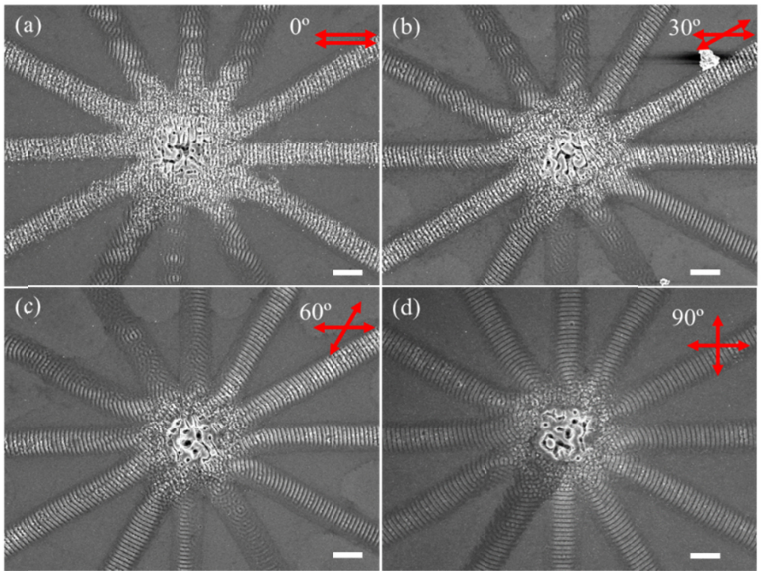

Fig. 2. SEM images of LIPSS fabricated at different double-pulse polarization angles: (a) 0°, (b) 30°, (c) 60°, and (d) 90°. The time delay was maintained at 1 ps and the peak laser fluence of each double pulse was maintained at 0.50 J/cm^2. The horizontally polarized pulse was always secondary to the other pulse. The double-arrow red lines indicate the laser polarization direction. Scale bar: 5 μm.

3.1 Orientation of LIPSS dependence on the angles between the two pulses polarizations and the scanning direction

Following the straight scanning path illustrated in Fig. **1**, we fabricated the LIPSS on silicon by applying different polarized and equal-energy femtosecond laser double-pulse trains. The angles between the two pulses polarizations were set to 0°, 30°, 60°, and 90°. The peak laser fluence of each of the double pulses was maintained at 0.50 J/cm^2, which was slightly lower than the peak single-pulse ablation threshold. Moreover, the laser repetition rate, scanning

Optics EXPRESS

speed, and time delay between the double pulses were maintained at 100 Hz, 150 μm/s, and 1 ps, respectively. Figure 2(a) depicts the results obtained when the angle between the two pulses polarizations was 0° (i.e., parallel polarized femtosecond double-pulse trains). In the scanning path in which the scanning direction was parallel or perpendicular to the laser polarization direction, the orientation of the fabricated LIPSS was perpendicular to the laser polarization. However, in the other scanning paths, the orientation of the LIPSS was no longer perpendicular to the laser polarization; this finding was similar to the observations of a previous study that applied single-pulse scanning [19]. We can see that the orientation of the LIPSS was no longer fixed and that it rotated by certain angles. This phenomenon was verified when the angles between the two pulses polarizations were 30° and 60°, as presented in Figs. 2(b) and 2(c), respectively. Remarkably, when the angle between the two pulses polarizations was 90° (i.e., orthogonally polarized femtosecond double-pulse trains), we observed a notable phenomenon where the orientation of the LIPSS was perpendicular to the scanning direction, regardless of changes in the scanning direction; this study was the first to report this phenomenon.

Inspired by the above phenomenon, this provides us with a feasible method for manipulating the orientation of LIPSS in real time. Figures 3(a)-3(d) display the results obtained for the straight scanning path of several special scanning direction; the angles between the scanning direction and positive direction of Y axis were as follows: 0°, 30°, 60°, and 90°. The X axis and Y axis is defined in Fig. 3(l). For the structures depicted in Figs. 3(a) and 3(d), the scanning direction was identical to the polarization direction of one of the orthogonally polarized double pulses. By contrast, for the structures presented in Figs. 3(b) and 3(c), the scanning direction differed from the polarization directions of the generated double pulses. As indicated by the results, the orientation of the LIPSS fabricated using orthogonally polarized femtosecond double-pulse trains was perpendicular to the scanning direction, regardless of the scanning direction. In addition to the straight scanning path, we applied a sine-curve scanning path (with a continually changing curvature) and circular scanning path (with a constant curvature) to investigate the dependence of the LIPSS orientation on the scanning direction. During the scanning processes, the polarization directions of the double pulses constantly remained orthogonal. Figures 3(e)-3(i) present the results obtained for the sine-curve scanning path, and Figs. 3(j) and 3(k) present the results obtained for the circular scanning path. As revealed by these figures, the orientation of the LIPSS remained perpendicular to the scanning direction, similar to the results in Figs. 3(a)-3(d). Therefore, we determined that the observed orientation was a universal phenomenon, regardless of whether straight or curved scanning paths were used. We observed that the LIPSS fabricated through the curved scanning paths was no longer straight. Figures 3(f)-3(i), present magnified views of regions I–IV depicted in Fig. 3(e), indicating that the curvature of the path affected the bending degree of the LIPSS. The bending degrees of the LIPSS in regions I and III were greater than those of the LIPSS in regions II and IV, where the structures were nearly straight owing to the near-zero curvature. We also observed that the order of the horizontally polarized pulse and vertically polarized pulse did not alter the overall results. Therefore, we present only the results obtained for the vertically polarized pulse ahead of the horizontally polarized pulse. According to the preceding results, changing the laser polarization state was unnecessary; therefore, we were able to easily and steadily manipulate the orientation of the LIPSS such that it was perpendicular to the scanning direction.

Optics EXPRESS

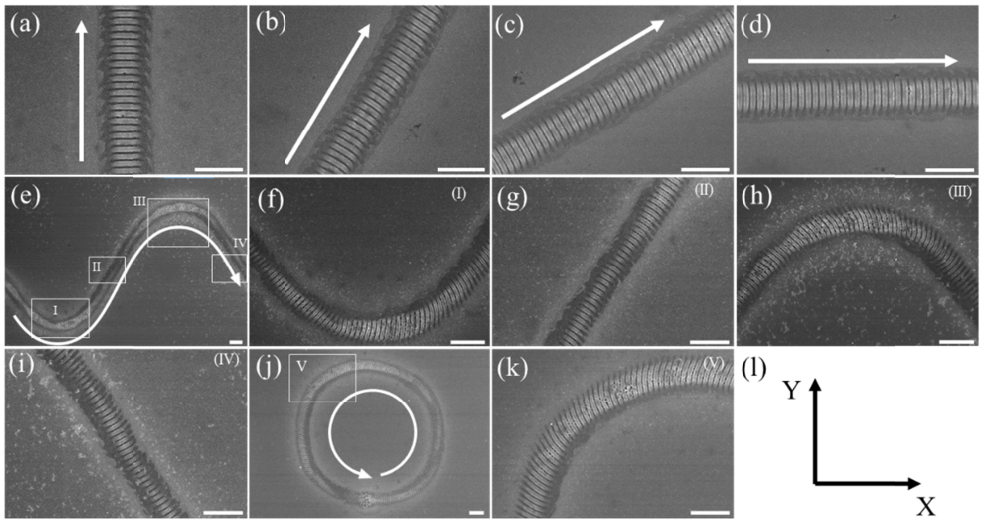

Fig. 3. (a)-(k) SEM images of LIPSS fabricated using orthogonally polarized femtosecond double-pulse trains. (l) The coordinate system used to determine the scanning direction. The white arrow lines indicate the scanning direction. Scale bar: 5 μm.

The periods of the fabricated LIPSS were carefully measured by two-dimensional fast Fourier transform (2D-FFT) to quantitatively examine their uniformity. Figure 4 illustrates the period of the LIPSS for straight scanning path as a function of the angle between the scanning direction and positive direction of Y axis, which ranged from 0° to 330°. The term "V+H" represents a situation where the vertically polarized pulse served as the leading pulse; the corresponding plot is indicated by the magenta curve with dots in the figure. Moreover, the term "H+V" represents a situation involving the opposite sequence. The fluctuations of the LIPSS periods for both the V + H and H + V situations were extremely minor, with an average period of approximately 730 nm in both situations. The ratio between the period range and mean period was 2% in both situations. The periods of the LIPSS fabricated in this study exhibited superior isotropy to those of LIPSS fabricated through single-pulse surface patterning [33].

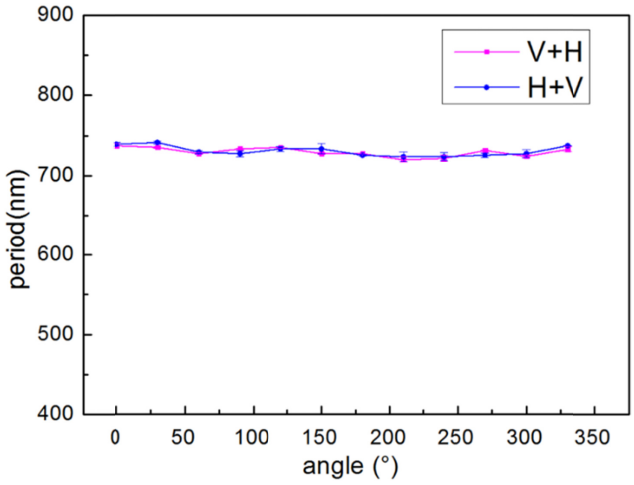

Fig. 4. Period of LIPSS in straight scanning as a function of the angle between the scanning direction and positive direction of Y axis, which ranged from 0° to 330°, "V+H" represents a

Optics EXPRESS

situation where the vertically polarized pulse served as the leading pulse while "H+V" represents a situation where the horizontally polarized pulse served as the leading pulse

3.2 Mechanism of LIPSS orientation perpendicular to the scanning direction

As mentioned, SPPs play a major role in the formation of LIPSS. SPPs are a type of wave emerging at the air and the excited silicon interface when the ionized free electron density reaches critical value [34]. And the SPPs are usually oriented along the laser polarization [30,31]. If SPPs being sufficiently strong, clear ordered continuous LIPSS can thus be formed. One study reported that in single-pulse surface patterning, LIPSS formation was more likely when the scanning direction approached the laser polarization direction [18], implying that the SPP intensity became stronger owing to the positive feedback process of grating-assisted SPPs-laser coupling enhancement effect [31]. In addition, SPPs exhibit evanescent decay and the wavevector of SPPs is along the laser polarization direction [35]. Therefore, in the case of surface scan processing, when the laser irradiation point is in the direction of wavevector of the SPPs, it is more benefit for the excitation and propagation of SPPs. Figures 5(a)-5(d) depict images of the structures fabricated using two special scanning directions in single-pulse surface patterning in the present study. The peak laser fluence in each case was 0.54 J/cm^2, which was slightly higher than the ablation threshold. Other parameters were the same as those used in the experiments involving orthogonally polarized double-pulse trains. It showed that for both the horizontally polarized and vertically polarized single-pulse surface scan processing, LIPSS came into being when the scanning direction was parallel to the laser polarization. By contrast, only a laser-modified zone was generated when the scanning direction was perpendicular to the laser polarization. In other words, the SPPs intensity changed with the angles between the scanning direction and laser polarization. The maximum intensity occurred at the angle 0°, and it was reduced to the minimum at the angle 90°, which was zero in our experiments. Considering the situation of exciting SPPs in a single spot, the electric field of the SPPs in the observing spot follows a cos (Θ) law [36], where Θ is the angle between the laser polarization and the line passing two spots above. Accordingly, we assume that the electric field of SPPs in single-pulse surface scan processing also follows a cos (Θ) law, with the electric field being correlated with SPPs intensity. Herein, a simple model is illustrated in Figs. 5(e)-5(g) to qualitatively analyze this phenomenon. The vector $\vec{E}$ represents the electric field of SPPs; its orientation is consistent with the direction of SPPs, same as the laser polarization, and its value matches the amplitude of the SPPs electric field. The blue arrows in Figs. 5(e)-5(g) represent the scanning direction and the double arrows indicate the laser polarization. E_0 represents the maximum amplitude of the SPPs excited by a single pulse when the scanning direction is parallel to the laser polarization. In horizontally polarized single-pulse scanning, the amplitude of the SPPs electric field $|\vec{E}_H|$ can be expressed as follows:

$$|\vec{E}_H| = E_0 \cos(\theta) \tag{1}$$

where θ is the angle between the horizontally laser polarization and scanning direction. In vertically polarized single-pulse scanning, the amplitude of the SPPs electric field $|\vec{E}_V|$ can be expressed as follows:

$$|\vec{E}_V| = E_0 \cos(\pi/2 - \theta) \tag{2}$$

Figure 5(g) shows that SPPs excited by orthogonally polarized double-pulse trains can be derived by summing the vectors of SPPs excited by horizontally polarized and vertically polarized pulses. In the direction perpendicular to the scanning path, the following formula can be obtained:

$$|\vec{E}_H|\sin(\theta) = |\vec{E}_V|\cos(\theta) \tag{3}$$

Optics EXPRESS

Hence, the SPPs excited by the orthogonally polarized double-pulse trains are oriented along the scanning direction. LIPSS can be formed through periodic deposition of energy along the direction of SPPs [30]. This explains why the orientation of the LIPSS fabricated on silicon by using the orthogonally polarized femtosecond double-pulse trains was perpendicular to the scanning direction. In addition,

$$|\vec{E}| = |\vec{E}_H|\cos(\theta) + |\vec{E}_V|\cos(\pi/2-\theta) = E_0 \quad (4)$$

This equation indicates that the amplitude of the electric field of the SPPs excited by the orthogonally polarized double-pulse trains remains constant, regardless of the scanning direction. Naturally, the absorption of laser pulse energy inherently remains constant in different scanning directions. That is, if other manufacturing parameters staying the same, the wavelength of the SPPs are the same along different scanning directions as well. This explains the considerable isotropy in the periods of the LIPSS fabricated through the orthogonally polarized femtosecond double-pulse trains in this study. In addition, for other double-pulse angles between two pulses polarizations, the direction of combined SPPs is no longer along the scanning direction, and the intensity of SPPs changes with the scanning direction. This explains why the orientation of the fabricated LIPSS was not perpendicular to the scanning direction [Figs. 2(a)-2(c)]. Besides, the uniformity of the LIPSS changed depending on the scanning direction [Figs. 2(a)-2(c)]. The ablation of the LIPSS was more severe in scanning directions that were closer to the laser polarization.

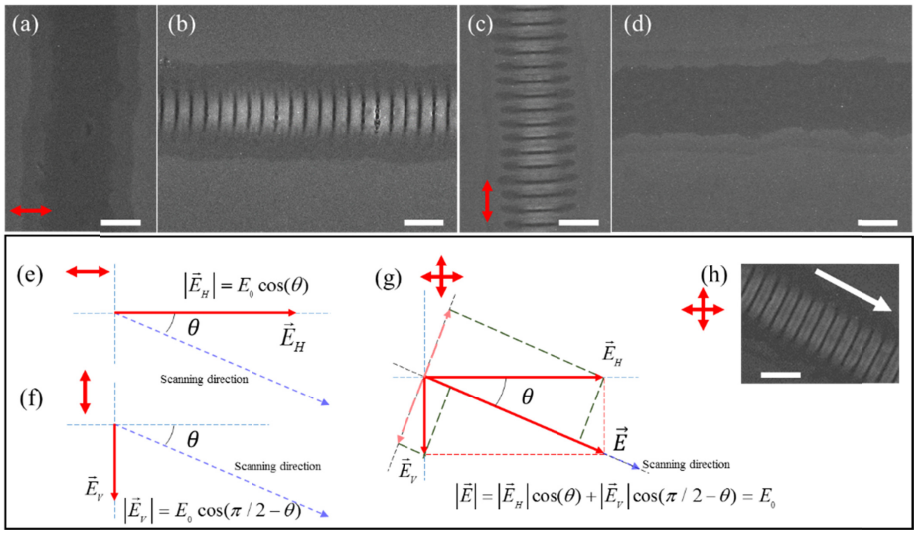

Fig. 5. (a), (b) SEM images of the structure fabricated using horizontally polarized single-pulse surface patterning. (c), (d) SEM images of the structure fabricated using vertically polarized single-pulse surface patterning. (e)- (g) A simple model depicting generation of SPPs in different laser polarization surface patterning processes. (h) SEM images of the structure fabricated using orthogonally polarized double-pulse trains. Scale bar, 2 μm.

The time delay between the double pulses was set to 1 ps. Other time delays were also investigated. Figure 6 presents images of the fabricated LIPSS. The peak laser fluence of each of the double pulses was maintained at 0.50 J/cm^2. To clarify the evolution of the LIPSS, we selected the scanning path that involved a 30° angle between the scanning direction and positive direction of Y axis. From the 2D-FFT of the SEM images, we got the angles between the LIPSS orientation and the scanning direction displayed by the angles in Fig. 6. The angles were 90° for time delay from 0fs to 5ps. For time delays of 10 ps, 12 ps, 50 ps, and 100 ps, the angles were approximately 91.7°, 91.7°, 93.4°, and 96.8°, respectively. We could see that for time delays longer than 10 ps (including 10 ps), the LIPSS orientation

Optics EXPRESS

was no longer perpendicular to the scanning direction. Moreover, the uniformity of the LIPSS morphology decreased as the time delay increased. The clearest and most uniform LIPSS were formed at a time delay of 1 ps. The lifetime of SPPs is typically on a sub picosecond scale and depends heavily on material and irradiation parameters [37]. To form new combined SPPs, SPPs stimulated by each sub pulse should coexist for vector addition before they diminish and disappear. Thus, the time delay between double pulses should be within an appropriate range. If a long time delay is used, the SPPs excited by two sub pulses do not match and the orientation of the combined SPPs is no longer parallel to the scanning direction; consequently, the orientation of the resulting LIPSS is not perpendicular to the scanning direction. Furthermore, if SPPs excited by subpulses can coexist, the order of horizontally polarized and vertically polarized pulses is negligible in the generation of LIPSS.

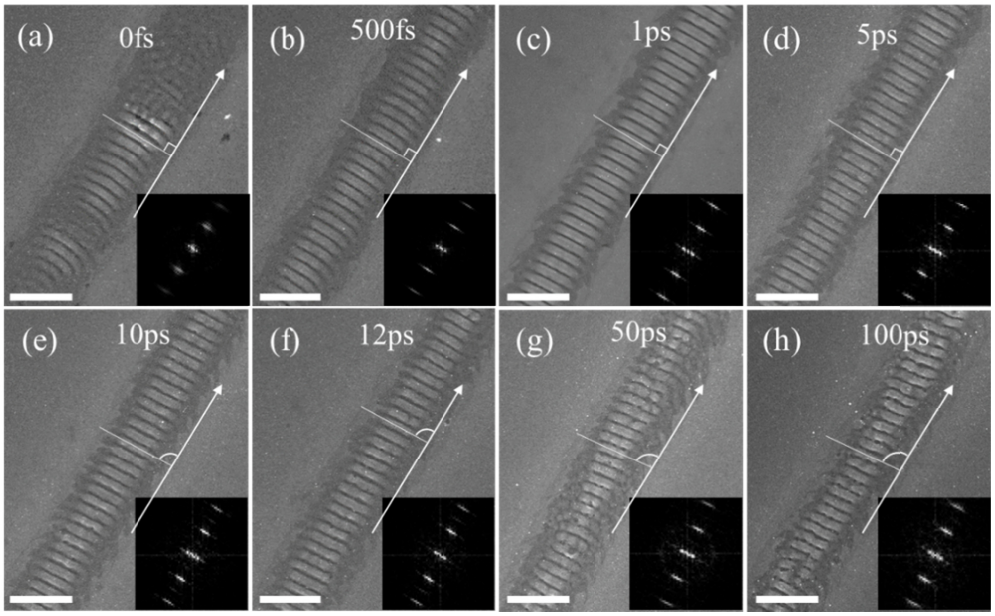

Fig. 6. Scanning electron microscope images of LIPSS fabricated using multiple time delays between double pulses: (a) 0 fs, (b) 500 fs, (c) 1 ps, (d) 5 ps, (e) 10 ps, (f) 12 ps, (g) 50 ps, and (h) 100 ps. The peak laser fluence of each of the double pulses was maintained at 0.50 J/cm^2. Scale bar: 4 μm.

3.3 An application of surface coloration

We revealed a phenomenon where the LIPSS orientation was constantly perpendicular to the scanning direction. This phenomenon demonstrated that we successfully developed a new method to manipulate the LIPSS orientation by using orthogonally polarized femtosecond laser double-pulse trains. Figure 7 displays the results obtained when we applied the proposed method to generate structural colors. By merely adjusting the scanning direction, we fabricated LIPSS with multiple orientations to serve as diffractive gratings in the separate regions illustrated in Figs. 7(a) and 7(e). When the gratings were vertically irradiated with white light, structural colors emerged. When the irradiation direction was parallel to the gratings, no structural colors were observed. Figures 7(b), 7(c), 7(f), and 7(g) present the structural colors observed under white light irradiation in a single direction. Figures 7(d) and 7(h) illustrate the different structural colors obtained under simultaneous white light irradiation in two individual directions. In traditional fabrication methods [38], the laser polarization direction must be rotated to fabricate LIPSS gratings with different orientations. However, in our proposed method, only one parameter, namely the scanning direction,

Optics EXPRESS

requires adjustment; this facilitates manipulation of the LIPSS orientation and considerably improves fabrication efficiency. Moreover, a ring pattern was fabricated through hundreds of circular scanning paths; for each scanning path, the fabricated LIPSS were perpendicular to the scanning direction and pointed toward the center of the circle, as presented in Fig. 7(i). The resulting structural colors are provided in Figs. 7(j)-7(l). Because the grating structures were not strictly parallel, the regions with structural colors were sector rings. Furthermore, relatively complicated surface patterns could be readily realized using a well-designed scanning path.

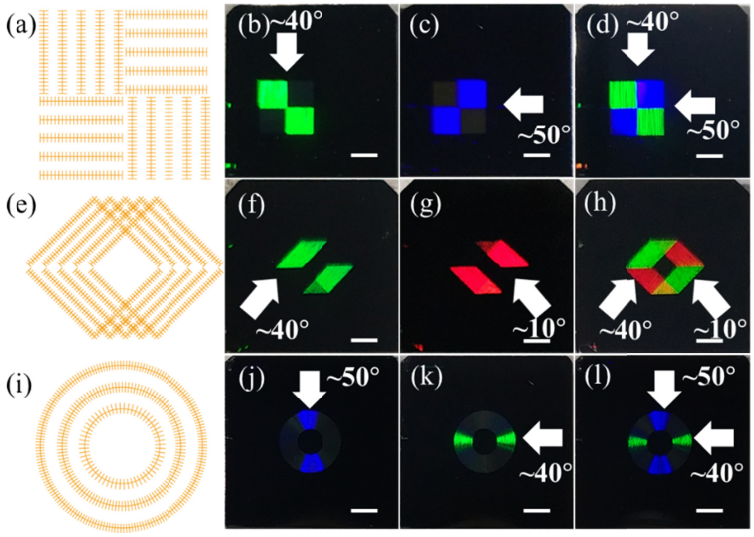

Fig. 7. Structural colors generated using the proposed method. (a), (e), and (i) Schematics of two fabrication plans for LIPSS gratings. (b), (c), (f), (g), (j), and (k) Observed structural colors under white light irradiation in only one direction. (d), (h), and (l) Observed structural colors under white light irradiation in two directions. The white arrows indicate the incident direction of white light. The angle values indicate the angles between white light and the horizontal line. Scale bar: 1.5 mm.

4. Conclusion

We developed a feasible and effective method for manipulating the orientation of LIPSS. By controlling the orientation of SPPs along the scanning direction by using orthogonally polarized and equal-energy femtosecond double-pulse trains with a time delay of 1 ps, we were able to manipulate the LIPSS orientation such that it was constantly perpendicular to the scanning direction, regardless of the applied scanning path. Compared with traditional fabrication methods, our method does not require complex rotating devices and affords an easier means of controlling the orientation of LIPSS; thus, this method constitutes a new strategy for laser surface fabrication. To demonstrate the functionality of our method, we applied it to generate structural colors.

Funding

National Key R&D Program of China (2018YFB1107200); National Natural Science Foundation of China (51675048); Beijing Natural Science Foundation (3194045); China Postdoctoral Science Foundation funded project (2018M630052; 2018-ZZ-017); Beijing Municipal Education Commission Foundation (KM201910005003).

References

1. S. H. Kong, D. D. L. Wijngaards, and R. F. Wolffenbuttel, "Infrared micro-spectrometer based on a diffraction grating," Sensor. Actuat. A-Phys. **92**(1–3), 88–95 (2001).

Optics EXPRESS

2. R. Dewan and D. Knipp, "Light trapping in thin-film silicon solar cells with integrated diffraction grating," J. Appl. Phys. **106**(7), 074901 (2009).
3. J. Neauport and N. Bonod, "Diffraction gratings: from principles to applications in high-intensity lasers," Adv. Opt. Photonics **8**(1), 156–199 (2016).
4. H. J. Cornelissen, D. K. G. de Boer, and T. Tukker, "Diffraction gratings for Lighting applications," Proc. SPIE **8835**, 88350I (2013).
5. H. Xie, Q. Wang, S. Kishimoto, and F. Dai, "Characterization of planar periodic structure using inverse laser scanning confocal microscopy Moiré method and its application in the structure of butterfly wing," J. Appl. Phys. **101**(10), 103511 (2007).
6. A. Sezginer, K. C. Johnson, and F. E. Stanke, "Overlay alignment metrology using diffraction gratings," (Google Patents, 2004).
7. C. A. Palmer and E. G. Loewen, *Diffraction grating handbook* (Newport Corporation, 2005).
8. J. Bonse, S. Höhm, S. V. Kirner, A. Rosenfeld, and J. Krüger, "Laser-induced periodic surface structures—a scientific evergreen," IEEE J. Sel. Top. Quantum Electron. **23**(3), 9000615 (2017).
9. T. Y. Hwang and C. L. Guo, "Angular effects of nanostructure-covered femtosecond laser induced periodic surface structures on metals," J. Appl. Phys. **108**(7), 073523 (2010).
10. J. Bonse and J. Kruger, "Pulse number dependence of laser-induced periodic surface structures for femtosecond laser irradiation of silicon," J. Appl. Phys. **108**(3), 034903 (2010).
11. S. Schwarz, S. Rung, C. Esen, and R. Hellmann, "Surface Plasmon Polariton Triggered Generation of 1D-Low Spatial Frequency LIPSS on Fused Silica," Appl. Sci. (Basel) **8**(9), 1624 (2018).
12. T. Jwad, P. Penchev, V. Nasrollahi, and S. Dimov, "Laser induced ripples' gratings with angular periodicity for fabrication of diffraction holograms," Appl. Surf. Sci. **453**, 449–456 (2018).
13. A. Cerkauskaite, R. Drevinskas, A. Solodar, I. Abdulhalim, and P. G. Kazansky, "Form-birefringence in ITO thin films engineered by ultrafast laser nanostructuring," ACS Photonics **4**(11), 2944–2951 (2017).
14. F. Liang, R. Vallée, and S. L. Chin, "Pulse fluence dependent nanograting inscription on the surface of fused silica," Appl. Phys. Lett. **100**(25), 251105 (2012).
15. P. Gregorčič, M. Sedlacek, B. Podgornik, and J. Reif, "Formation of laser-induced periodic surface structures (LIPSS) on tool steel by multiple picosecond laser pulses of different polarizations," Appl. Surf. Sci. **387**, 698–706 (2016).
16. R. Le Harzic, D. Dörr, D. Sauer, M. Neumeier, M. Epple, H. Zimmermann, and F. Stracke, "Large-area, uniform, high-spatial-frequency ripples generated on silicon using a nanojoule-femtosecond laser at high repetition rate," Opt. Lett. **36**(2), 229–231 (2011).
17. E. Rebollar, S. Pérez, J. J. Hernández, I. Martín-Fabiani, D. R. Rueda, T. A. Ezquerra, and M. Castillejo, "Assessment and formation mechanism of laser-induced periodic surface structures on polymer spin-coated films in real and reciprocal space," Langmuir **27**(9), 5596–5606 (2011).
18. P. Liu, L. Jiang, J. Hu, W. Han, and Y. Lu, "Direct writing anisotropy on crystalline silicon surface by linearly polarized femtosecond laser," Opt. Lett. **38**(11), 1969–1971 (2013).
19. P. Liu, L. Jiang, J. Hu, S. Zhang, and Y. Lu, "Self-organizing microstructures orientation control in femtosecond laser patterning on silicon surface," Opt. Express **22**(14), 16669–16675 (2014).
20. G. Giannuzzi, C. Gaudiuso, C. Di Franco, G. Scamarcio, P. M. Lugara, and A. Ancona, "Large area laser-induced periodic surface structures on steel by bursts of femtosecond pulses with picosecond delays," Opt. Lasers Eng. **114**, 15–21 (2019).
21. M. Shen, J. E. Carey, C. H. Crouch, M. Kandyla, H. A. Stone, and E. Mazur, "High-density regular arrays of nanometer-scale rods formed on silicon surfaces via femtosecond laser irradiation in water," Nano Lett. **8**(7), 2087–2091 (2008).
22. M. Barberoglou, G. D. Tsibidis, D. Gray, E. Magoulakis, C. Fotakis, E. Stratakis, and P. A. Loukakos, "The influence of ultra-fast temporal energy regulation on the morphology of Si surfaces through femtosecond double pulse laser irradiation," Appl. Phys., A Mater. Sci. Process. **113**(2), 273–283 (2013).
23. S. Höhm, M. Rohloff, A. Rosenfeld, J. Krüger, and J. Bonse, "Dynamics of the formation of laser-induced periodic surface structures on dielectrics and semiconductors upon femtosecond laser pulse irradiation sequences," Appl. Phys., A Mater. Sci. Process. **110**(3), 553–557 (2013).
24. F. Fraggelakis, E. Stratakis, and P. A. Loukakos, "Control of periodic surface structures on Silicon by combined temporal and polarization shaping of femtosecond laser pulses," Appl. Surf. Sci. **444**, 154–160 (2018).
25. S. Höhm, M. Herzlieb, A. Rosenfeld, J. Krüger, and J. Bonse, "Femtosecond laser-induced periodic surface structures on silicon upon polarization controlled two-color double-pulse irradiation," Opt. Express **23**(1), 61–71 (2015).
26. B. Dusser, Z. Sagan, H. Soder, N. Faure, J. P. Colombier, M. Jourlin, and E. Audouard, "Controlled nanostructrures formation by ultra fast laser pulses for color marking," Opt. Express **18**(3), 2913–2924 (2010).
27. E. Skoulas, A. Manousaki, C. Fotakis, and E. Stratakis, "Biomimetic surface structuring using cylindrical vector femtosecond laser beams," Sci. Rep. **7**(1), 45114 (2017).
28. K. Lou, S. X. Qian, X. L. Wang, Y. Li, B. Gu, C. Tu, and H. T. Wang, "Two-dimensional microstructures induced by femtosecond vector light fields on silicon," Opt. Express **20**(1), 120–127 (2012).
29. T. J. Derrien, J. Krüger, T. E. Itina, S. Höhm, A. Rosenfeld, and J. Bonse, "Rippled area formed by surface plasmon polaritons upon femtosecond laser double-pulse irradiation of silicon," Opt. Express **21**(24), 29643–29655 (2013).

Optics EXPRESS

30. L. Wang, Q. D. Chen, X. W. Cao, R. Buividas, X. Wang, S. Juodkazis, and H. B. Sun, "Plasmonic nano-printing: large-area nanoscale energy deposition for efficient surface texturing," Light Sci. Appl. **6**(12), e17112 (2017).
31. M. Huang, F. Zhao, Y. Cheng, N. Xu, and Z. Xu, "Origin of laser-induced near-subwavelength ripples: interference between surface plasmons and incident laser," ACS Nano **3**(12), 4062–4070 (2009).
32. J. M. Liu, "Simple technique for measurements of pulsed Gaussian-beam spot sizes," Opt. Lett. **7**(5), 196–198 (1982).
33. V. Stankevič, G. Račiukaitis, F. Bragheri, X. Wang, E. G. Gamaly, R. Osellame, and S. Juodkazis, "Laser printed nano-gratings: orientation and period peculiarities," Sci. Rep. **7**(1), 39989 (2017).
34. H. Raether, *Surface-Plasmons on Smooth and Rough Surfaces and on Gratings* (Springer, 1986).
35. V. V. Gerasimov, B. A. Knyazev, I. A. Kotelnikov, A. K. Nikitin, V. S. Cherkassky, G. N. Kulipanov, and G. N. Zhizhin, "Surface plasmon polaritons launched using a terahertz free-electron laser: propagation along a gold-ZnS-air interface and decoupling to free waves at the surface edge," J. Opt. Soc. Am. B **30**(8), 2182–2190 (2013).
36. A. Drezet, A. L. Stepanov, H. Ditlbacher, A. Hohenau, B. Steinberger, F. R. Aussenegg, A. Leitner, and J. R. Krenn, "Surface plasmon propagation in an elliptical corral," Appl. Phys. Lett. **86**(7), 074104 (2005).
37. T. J. Y. Derrien, J. Krüger, and J. Bonse, "Properties of surface plasmon polaritons on lossy materials: lifetimes, periods and excitation conditions," J. Opt. **18**(11), 115007 (2016).
38. J. Yao, C. Zhang, H. Liu, Q. Dai, L. Wu, S. Lan, A. V. Gopal, V. A. Trofimov, and T. M. Lysak, "Selective appearance of several laser-induced periodic surface structure patterns on a metal surface using structural colors produced by femtosecond laser pulses," Appl. Surf. Sci. **258**(19), 7625–7632 (2012).